ACS OMEGA

http://pubs.acs.org/journal/acsodf

Article

Theoretical Study of the Gas-Phase Hydrolysis of Formaldehyde to Produce Methanediol and Its Implication to New Particle Formation

Chunyu Wang, Xiaoju Chen, Yirong Liu, Teng Huang, and Shuai Jiang*

Cite This: *ACS Omega* 2023, 8, 15467−15478

Read Online

ACCESS | Metrics & More | Article Recommendations | Supporting Information

ABSTRACT: Aldehydes were speculated to be important precursor species in new particle formation (NPF). The direct involvement of formaldehyde (CH_2O) in sulfuric acid and water nucleation is negligible; however, whether its atmospheric hydrolysate, methanediol ($CH_2(OH)_2$), which contains two hydroxyl groups, participates in NPF is not known. This work investigates both CH_2O hydrolysis and NPF from sulfuric acid and $CH_2(OH)_2$ with quantum chemistry calculations and atmospheric cluster dynamics modeling. Kinetic calculation shows that reaction rates of the gas-phase hydrolysis of CH_2O catalyzed by sulfuric acid are 11−15 orders of magnitude faster than those of the naked path at 253−298 K. Based on structures and the calculated formation Gibbs free energies, the interaction between sulfuric acid/its dimer/its trimer and $CH_2(OH)_2$ is thermodynamically favorable, and $CH_2(OH)_2$ forms hydrogen bonds with sulfuric acid/its dimer/its trimer via two hydroxyl groups to stabilize clusters. Our further cluster kinetic calculations suggested that the particle formation rates of the system are higher than those of the binary system of sulfuric acid and water at ambient low sulfuric acid concentrations and low relative humidity. In addition, the formation rate is found to present a negative temperature dependence because evaporation rate constants contribute significantly to it. However, cluster growth is essentially limited by the weak formation of the largest clusters, which implies that other stabilizing vapors are required for stable cluster formation and growth.

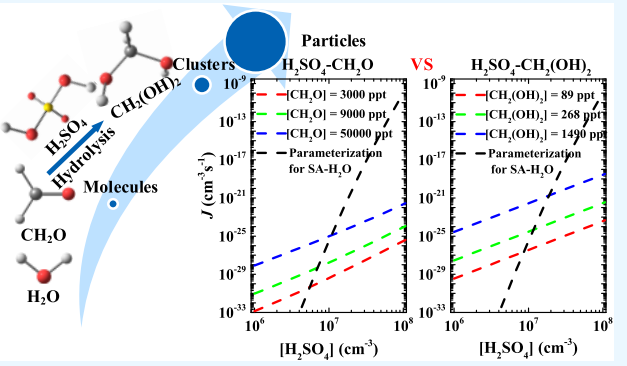

1. INTRODUCTION

New particle formation (NPF) is the source of over half of the atmospheric cloud condensation nuclei, thus influencing cloud properties and Earth's energy balance.[1] Nucleated particles include the formation of stabilized clusters and their subsequent growth. However, the chemical identity and relative significance of the participating vapors remain highly uncertain. Experiments performed at the CLOUD chamber have shown that NPF from sulfuric acid and strong bases, such as dimethylamine, correlates well with atmospheric observations,[2] but their concentrations are not enough to explain the particle nucleation rates and growth rates under atmospheric conditions,[3−5] and other organic nucleation candidates play important roles in particle formation and the subsequent growth stages.[6−10]

Formaldehyde (CH_2O) is the simplest but most abundant (approximately 70−80%) carbonyl compound in the atmosphere,[11] ranging from thousands of pptv to dozens of ppbv observed in different areas of the world,[12−14] and it is typically present at concentrations equal to that of all other aldehyde species combined in cloudwater.[15−17] It is of special concern because it is an important intermediate product of photochemical reactions in the atmosphere, and it has a certain role in atmospheric reactivity and oxidizing ability.[11,18−20] Globally, the main source of formaldehyde in clean and remote areas is the photochemical oxidation of CH_4, but in rural areas, the oxidation of hydrocarbons emitted by natural sources (such as terpenes and isoprene) and man-made sources is also a source of CH_2O.[21] Previous investigations have suggested that the major sink processes of CH_2O in gas-phase atmospheric chemistry are photolysis[22,23] and reaction with the hydroxyl radical,[24] which produces HO_X radicals.[25,26] Budget analyses of CH_2O reveal large discrepancies between observed CH_2O concentrations and those predicted from models.[27,28] Recently, gas-phase hydrolysis of CH_2O,[29,30] uptake of CH_2O by aerosols/clouds,[31−33] soil surfaces,[34] and direct participation of CH_2O in nucleation[35,36] have been of great interest, which could present additional CH_2O sink pathways and thus reduce overestimation of CH_2O.

Previous studies have shown that formaldehyde and the products of aldehyde heterogeneous reactions, including hydrolysis, can contribute to the formation and growth of

Received: February 6, 2023
Accepted: March 30, 2023
Published: April 21, 2023

secondary organic aerosols (SOAs).[35,37,38] However, our previous simulations of cluster growth flux and flow tube experiments show that CH_2O with H_2SO_4 clustering is weak and that the enhancement of CH_2O in H_2SO_4-H_2O homogeneous nucleation is negligible. A previous study showed that gas-phase CH_2O hydrolysis to form methanediol ($CH_2(OH)_2$) does not take place due to the extremely high energy barrier in the atmosphere.[39−41] Nevertheless, experiments[42,43] have shown that the hydrolysis of aldehydes could occur under conditions corresponding to a water-restricted gas-phase environment. In addition, some studies have also demonstrated that atmospheric acids can significantly lower the barrier of these hydrolysis reactions, including sulfuric acid,[29,44] formic acid,[44,45] nitric acid[45] and oxalic acid,[45] where they act as bridges for hydrogen atom transfer. However, they either did not generalize the effective reaction rate from monomers or did not compare the reaction rate to other major sink rates, or none of the above. The kinetics of the hydrolysis of CH_2O are still limited, and the potential for subsequent participation in NPF is unknown.

From the perspective of its structure, $CH_2(OH)_2$ possesses two hydroxyl functional groups, which can act as hydrogen donors to interact with atmospheric particle precursors and thus promote NPF.[35,46] Recently, Shi et al.[35] used quantum chemical calculations to elucidate the possibility of aldehydes as well as the hydration products with sulfuric acid forming clusters in atmospheric particle formation. Hence, the CH_2O hydrolysis reaction may play a positive role in NPF, which is helpful to better understand the atmospheric CH_2O reactions and is also important to assess the effects of geminal diol on NPF.

In this study, we examine the catalytic effect of sulfuric acid (SA) on the CH_2O hydrolysis to produce $CH_2(OH)_2$ and comparatively investigate the formation of molecular clusters of SA and CH_2O, SA and $CH_2(OH)_2$ using a combination of quantum chemical calculations and kinetic modeling employing the Atmospheric Cluster Dynamics Code (ACDC).[47,48] Via systematic conformational searches, we obtained minimum Gibbs free energy structures of clusters of composition $(H_2SO_4)_m(B)_n$ ($0 \le m, n \le 3$; "B" represents CH_2O or $CH_2(OH)_2$). The corresponding thermodynamic data are used in ACDC to obtain cluster steady-state concentrations and formation rates of particles. In addition, the effects of temperature and vapor concentration on cluster formation are considered. The logic of this work is whether the hydrolysis of CH_2O can serve as a loss pathway for CH_2O and whether its hydrolysate can participate in NPF under atmospheric conditions.

2. COMPUTATIONAL METHODS

2.1. Quantum Chemical Calculations. The basin-hopping (BH) algorithm[49−51] coupled with the PM7 semi-empirical potential[52] implemented in the MOPAC 2016 program (http://openmopac.net) was employed to search for the initial geometries. This BH method has been validated to perform well for both atomic and molecular systems in our previous studies.[53−58] Then, the top 20 lowest-lying conformers of each species were optimized at the PW91PW91/6-311++G(3df,3pd) level to determine the final configurations with the Gaussian 09 software package.[59] Harmonic vibrational frequencies were calculated to confirm that the obtained conformers were the true minima. The method provides good geometries,[60,61] excellent vibrational frequencies,[62] and quite accurate cluster Gibbs free energies compared with the currently available experiments.[58,63,64] Based on PW91PW91/6-311++G(3df,3pd)-optimized geometries and frequencies (i.e., the $\Delta G_{thermal}$ contribution), single-point energy calculations for the $(H_2SO_4)_m(B)_n$ ($0 \le m, n \le 3$; "B" represents CH_2O or $CH_2(OH)_2$) clusters were carried out using DLPNO-CCSD(T)/aug-cc-pVTZ with the ORCA 4.0 suite of programs.[65] The approximate $\Delta G_{bind}^{CCSD(T)}$ (hereafter, ΔG) value is calculated from the binding energy (ΔE) and the $\Delta G_{thermal}$ contribution as follows

$$\Delta G_{bind}^{CCSD(T)} = \Delta E^{CCSD(T)} + \Delta G_{thermal}^{DFT} \quad (1)$$

2.2. Kinetics Calculations. For kinetic calculations, geometrical structures of all reactants, prereaction complexes, transition states, postreaction complexes, and products were optimized using the M06-2X[66] method in conjunction with the 6-311++G(d,p)[67] basis set. To refine the relative energies of the various stationary points, single-point energy calculations were also carried out at the DLPNO-CCSD(T)/aug-cc-pVTZ level of theory. To evaluate the effects of SA on the rate constants of the gas-phase CH_2O hydrolysis reaction, the reaction rate constants are evaluated based on conventional transition-state theory (TST) with Eckart tunneling correction[68,69] at the DLPNO-CCSD(T)/aug-cc-pVTZ//M06-2X/6-311++G(d,p) level and executed with the KiSThelP program.[70]

The formation of $CH_2(OH)_2$ from CH_2O and H_2O is described as follows

$$CH_2O + H_2O \rightleftharpoons (CH_2O)(H_2O) \quad (2)$$

$$(CH_2O)(H_2O) \rightarrow CH_2(OH)_2 \quad (3)$$

Applying the steady-state approximation to the prereactive complex and assuming that the complex is in equilibrium with the reactant, the uncatalyzed formation reaction rate of $CH_2(OH)_2$ (ν_{un}) can be described as eq 4[29]

$$\nu_{un} = \frac{d[CH_2(OH)_2]}{dt} = \frac{k_2}{k_{-2}} \times k_3[CH_2O][H_2O] = K_{(CH_2O)(H_2O)} \times k_3 \times [CH_2O][H_2O] \quad (4)$$

$$k_{un} = K_{(CH_2O)(H_2O)} \times k_3 \quad (5)$$

In the above equations, $K_{(CH_2O)(H_2O)}$ is the equilibrium constant for eq 2. k_2 and k_3 are the forward rate constants for eqs 2 and 3, respectively. k_{-2} is the reverse rate constant for eq 2. k_{un} is the rate constant of the formaldehyde hydrolysis without a catalyst.

In the presence of the catalyst H_2SO_4, the reaction proceeds via collision with each other to form dimers, and then the dimers encounter the third reactant to form the $(CH_2O)(H_2O)(H_2SO_4)$ complex, which is followed by unimolecular transformation to form $(CH_2(OH)_2)(H_2SO_4)$ complex in the exit channel. H_2SO_4 can participate in the atmospheric hydrolysis of CH_2O either by directly colliding with a $(CH_2O)(H_2O)$ complex or by having a CH_2O molecule collide with a $(H_2SO_4)(H_2O)$ complex. The two pathways can be expressed as

$$CH_2O + H_2O \rightleftharpoons (CH_2O)(H_2O) \quad (6)$$

$$(CH_2O)(H_2O) + H_2SO_4 \rightarrow CH_2(OH)_2 + H_2SO_4 \quad (7)$$

https://doi.org/10.1021/acsomega.3c00770
ACS Omega 2023, 8, 15467−15478

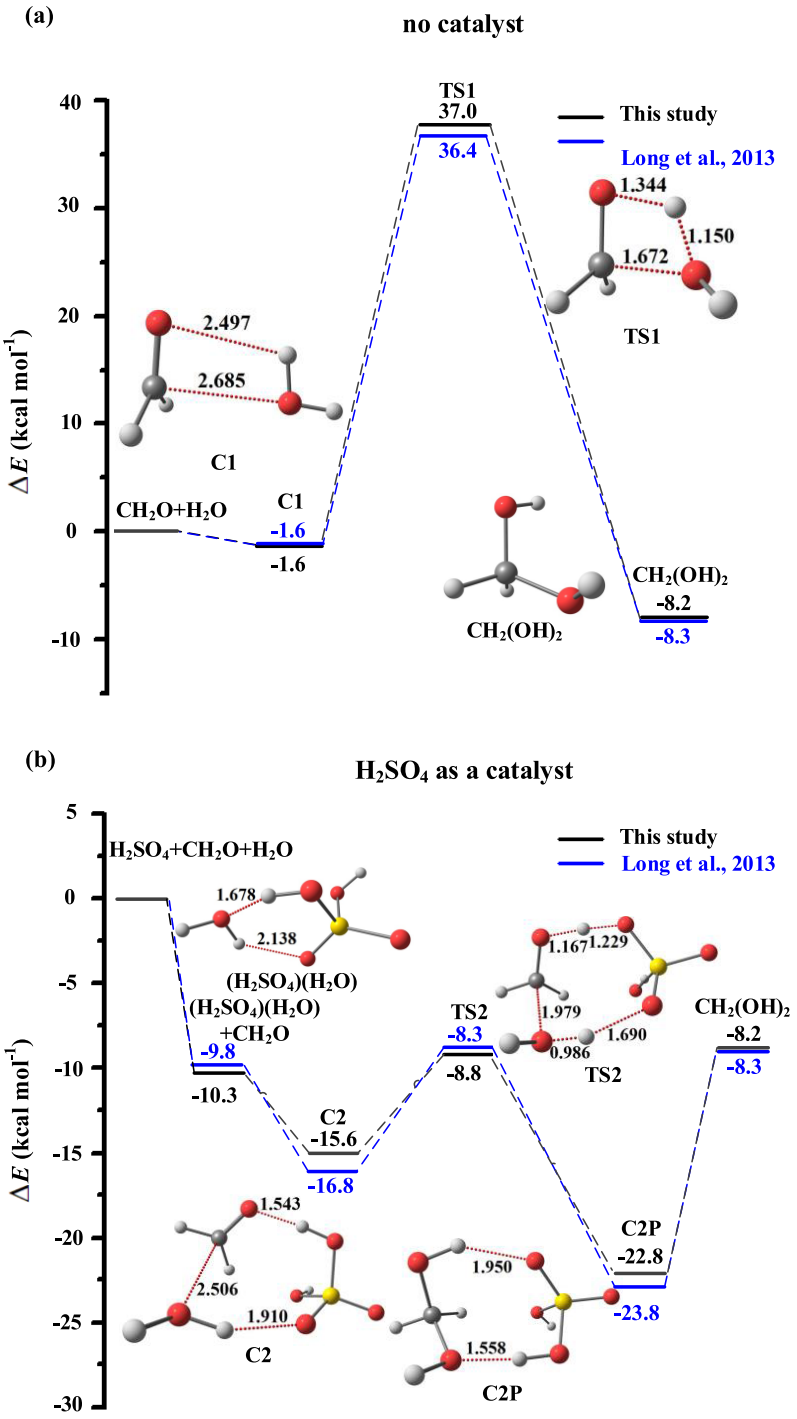

Figure 1. Potential energy surfaces with zero-point vibrational energies corrected at the DLPNO-CCSD(T)/aug-cc-pVTZ//M06-2X/6-311++G(d,p) level of theory (in kcal mol^{-1}) for the reaction of CH_2O + H_2O with (a) no catalyst and (b) H_2SO_4 as a catalyst.

and

$$H_2SO_4 + H_2O \rightleftharpoons (H_2SO_4)(H_2O) \quad (8)$$

$$CH_2O + (H_2SO_4)(H_2O) \rightarrow CH_2(OH)_2 + H_2SO_4 \quad (9)$$

For the path associated with the $(CH_2O)(H_2O)$ + H_2SO_4 reactants, applying the steady-state approximation to the prereactive complex and assuming that the complex is in equilibrium with the reactant, similar to the formation of H_2SO_4[71] and organic nitrate,[72] the H_2SO_4-catalyzed formation reaction rate of $CH_2(OH)_2$ ($\nu_{H_2SO_4}$) can be described as eq 10

$$\nu_{H_2SO_4} = \frac{d[CH_2(OH)_2]}{dt} = K_{(CH_2O)(H_2O)} \times k_7 \times [H_2SO_4][CH_2O][H_2O] \quad (10)$$

k_7 represents the bimolecular rate constant of the (CH_2O)-(H_2O) + H_2SO_4 reaction, which has been calculated using conventional transition-state theory with Eckart tunneling. The overall rate constant of the H_2SO_4-catalyzed formaldehyde hydrolysis (k_{eff,H_2SO_4}) is represented by eq 11

https://doi.org/10.1021/acsomega.3c00770
ACS Omega 2023, 8, 15467−15478

Table 1. Equilibrium Constants ($K_{(CH_2O)(H_2O)}$ and $K_{(H_2SO_4)(H_2O)}$, cm^3 molecules^{-1}), the Reaction Rate Coefficients (k_3, s^{-1}; k_9, k_{un} and k'_{eff}, cm^3 molecule^{-1} s^{-1}), and the Reaction Rates (v_{un} and v'_{eff}, molecules cm^{-3} s^{-1}) for the Formation of $CH_2(OH)_2$ from the Hydrolysis of Formaldehyde without/with Catalyzed Sulfuric Acid Calculated at the DLPNO-CCSD(T)/aug-cc-pVTZ//M06-2X/6-311++G(d,P) Level in the Temperature Range 253−298 K

M	253 K	263 K	273 K	283 K	298 K
$K_{(CH_2O)(H_2O)}$	3.58×10^{-23}	3.24×10^{-23}	2.96×10^{-23}	2.73×10^{-23}	2.45×10^{-23}
k_3	1.93×10^{-19}	9.91×10^{-19}	5.02×10^{-18}	2.42×10^{-17}	2.49×10^{-16}
$K_{(H_2SO_4)(H_2O)}$	2.65×10^{-17}	1.20×10^{-17}	5.73×10^{-18}	2.90×10^{-18}	1.14×10^{-18}
k_9	9.57×10^{-17}	1.03×10^{-16}	1.10×10^{-16}	1.17×10^{-16}	1.29×10^{-16}
k_{un}	6.92×10^{-42}	3.21×10^{-41}	1.48×10^{-40}	6.60×10^{-40}	6.11×10^{-39}
k'_{eff} [a]	2.53×10^{-26}	1.23×10^{-26}	6.31×10^{-27}	3.40×10^{-27}	1.47×10^{-27}
k_{OH} [b]	9.21×10^{-12}	9.02×10^{-12}	8.85×10^{-12}	8.70×10^{-12}	8.49×10^{-12}
v'_{eff}/v_{un} [c]	3.66×10^{15}	3.83×10^{14}	4.25×10^{13}	5.16×10^{12}	2.40×10^{11}
v'_{eff}/v_{OH} [d]	2.75×10^{-2}	1.36×10^{-2}	7.12×10^{-3}	3.91×10^{-3}	1.73×10^{-3}

[a] $[H_2SO_4]$ is 10^7 molecules cm^{-3}. [b] experimental rate constant from ref 63. [c] $[H_2SO_4]$ is 10^7 molecules cm^{-3}. [d] $[H_2O]$ and [OH] are 10^{18} and 10^5 molecules cm^{-3}, respectively.

$$k_{eff,H_2SO_4} = K_{(CH_2O)(H_2O)} \times k_7 \times [H_2SO_4] \quad (11)$$

For the path associated with the CH_2O + $(H_2SO_4)(H_2O)$ reactants, analogous to eqs 4 and 5, the rate expression and the rate constant for $CH_2(OH)_2$ formation can be written as eqs 12 and13

$$\nu'_{H_2SO_4} = K_{(H_2SO_4)(H_2O)} \times k_9 \times [H_2SO_4][CH_2O][H_2O] \quad (12)$$

$$k'_{eff,H_2SO_4} = K_{(H_2SO_4)(H_2O)} \times k_9 \times [H_2SO_4] \quad (13)$$

According to the ratio of the rate expressions for the two pathways shown in Text S1 and Table S1 in the Supporting Information (SI), CH_2O hydrolysis via the CH_2O + (H_2SO_4)-(H_2O) pathway is faster than that of the $(CH_2O)(H_2O)$ + H_2SO_4 reaction because the formation of the $(H_2SO_4)(H_2O)$ complex is more favorable than the $(CH_2O)(H_2O)$ complex.

We used the ACDC to study the formation rates and evaporation properties of clusters. The code generates and solves the cluster birth−death equations, the time derivatives of the concentrations of all constituents included in the simulation as eq 14

$$\frac{dc_i}{dt} = \frac{1}{2}\sum_{j<i} \beta_{j,(i-j)} c_j c_{(i-j)} + \sum_j \gamma_{(i+j)\to i} c_{i+j} - \sum_j \beta_{i,j} c_i c_j - \frac{1}{2}\sum_{j<i} \gamma_{i\to j} c_i + Q_i - S_i \quad (14)$$

where c_i is the concentration of cluster i, $\beta_{i,j}$ is the collision coefficient of clusters i with j, and $\gamma_{i+j\to j}$ is the evaporation coefficient of cluster $i + j$ evaporating into clusters i and j. Q_i is the possible additional source of cluster i, and S_i is the sink term of cluster i. The collision rate constants were calculated from the kinetic gas theory, and the evaporation rate constants were calculated from the Gibbs free energies of formation of the clusters according to the concept of detailed balance.

$$\gamma_{(i+j)\to i} = \beta_{ij} \frac{c_i^e c_j^e}{c_{i+j}^e} = \beta_{ij} c_{ref} \exp\left(\frac{\Delta G_{i+j} - \Delta G_i - \Delta G_j}{k_b T}\right) \quad (15)$$

Where c_i^e is the equilibrium concentration of cluster i, ΔG_i is the Gibbs free energy of the formation of cluster i, and c_{ref} is the monomer concentration of the reference vapor corresponding to the pressure of 1 atm at which the Gibbs free energies were determined.

In addition, the cluster formation rate in our study is defined as the flux of clusters outside the "3 × 3 box" system, where 3 is the maximum number of H_2SO_4, CH_2O, or $CH_2(OH)_2$ in the clusters, assuming the clusters on the boundaries are large enough to have negligible evaporation coefficients, since these clusters are not allowed to re-enter, it is as if they have become stable particles. A constant coagulation sink coefficient (sink term) and the source rate were set to zero for simplicity.

3. RESULTS AND DISCUSSION

3.1. Hydrolysis of Formaldehyde Without/With Catalyzed Sulfuric Acid. The reaction between formaldehyde and water produces a geminal diol, which is not photolabile in the atmosphere[73] and is expected to be more hygroscopic than formaldehyde due to its increased oxygen functionalization.[74] Gas-phase electronic structure calculations predict that two conformers of methanediol, cis-$CH_2(OH)_2$ and trans-$CH_2(OH)_2$, are thermodynamically favorable. Trans-$CH_2(OH)_2$ is more stable than cis-$CH_2(OH)_2$ because the distance between the hydrogen atoms of the hydroxyls in trans-$CH_2(OH)_2$ is longer than that in cis-$CH_2(OH)_2$, as shown in Figure S1 in the SI. From now on, we regard a trans-$CH_2(OH)_2$ as a methanediol if not specified.

As shown in Figure 1a, the fairly high reaction barrier resulting in the direct hydrolysis of formaldehyde without a catalyst is not a plausible path for $CH_2(OH)_2$ formation. The energy barrier is calculated to be 38.6 kcal mol^{-1} with respect to the prereactive complex, consistent with the previous value of 38.0 kcal mol^{-1}.[29] A large ring tension of the rather closed four-membered ring is in the transition-state (TS1) geometry, making the path kinetically unfavorable. For the reaction catalyzed by sulfuric acid (Figure 1b), the reactants are regarded as beginning with the formation of the (H_2SO_4)-(H_2O) complex and through a transition state (TS2) to lead to the formation of $CH_2(OH)_2$, as seen in the Section 2. The energy barrier is calculated to be 1.5 kcal mol^{-1} with respect to the reactants CH_2O and $(H_2SO_4)(H_2O)$, and it is clear that the reaction energy barrier of formaldehyde with water catalyzed by sulfuric acid is reduced by 37.1 kcal, which indicates that sulfuric acid exerts a strong catalytic effect on the hydrolysis of CH_2O.

https://doi.org/10.1021/acsomega.3c00770
ACS Omega 2023, 8, 15467−15478

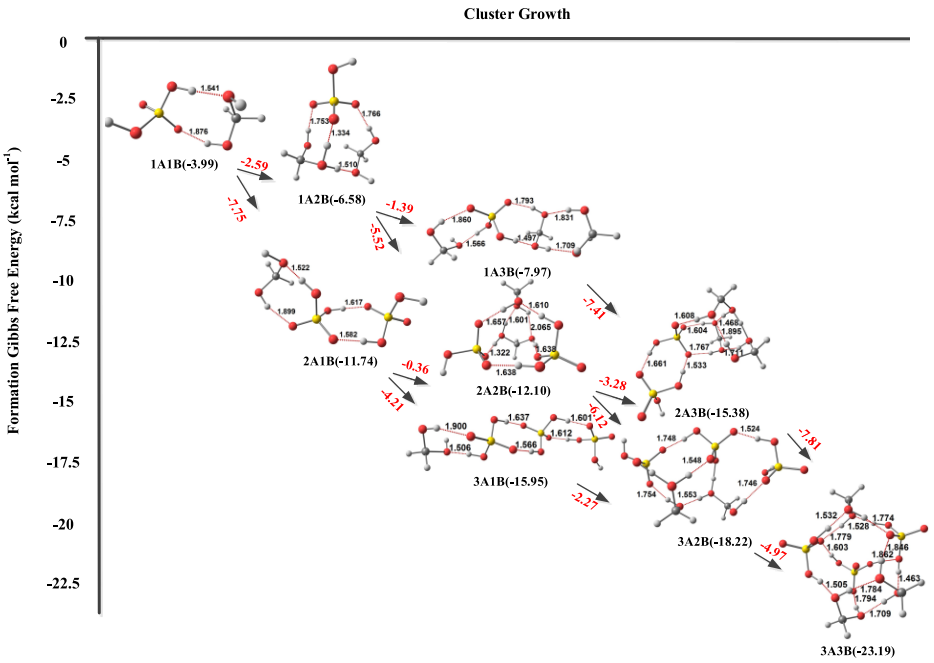

Figure 2. Diagram for the studied cluster formation steps, with structures of global Gibbs free energy minima obtained at the DLPNO-CCSD(T)/aug-cc-pVTZ//PW91PW91/6-311++G(3df,3pd) level of theory, in the $(H_2SO_4)_m(CH_2(OH)_2)_n$ (m = 1−3, n = 1−3) system. All presented values are the calculated Gibbs free energy changes, and the values in parentheses are the formation Gibbs free energies from monomers in kcal mol^{-1} at 298.15 K and 1 atm. Hydrogen bonds with bond lengths (Å) of each cluster are indicated.

The atmospheric implications of the studied reactions would be determined by how fast different reaction channels are and how they compete against each other; the reaction rate constants are then calculated here. The rate constants for each channel and equilibrium constants over the temperature range of 253−298 K are presented in Table 1. Without considering the catalyst, the rate constant k_{un} is 6.92×10^{-42} to 6.11×10^{-39} cm^3 molecule^{-1} s^{-1} at 253−298 K, which is too small for the reaction to occur. In the H_2SO_4 catalytic channel, the reaction rate constant is 2.53×10^{-26} to 1.47×10^{-27} cm^3 molecule^{-1} s^{-1} at a typical atmospheric $[H_2SO_4]$ of 10^7 molecules cm^{-3}, where the H_2SO_4 concentrations examined in the atmosphere span a wide range from 10^4 to 10^9 molecules cm^{-3}.[1,75] To obtain a more complete knowledge of the sulfuric acid effect in the CH_2O hydrolysis reaction, it is necessary to compare the rate of the naked and sulfuric acid-assisted reactions rather than comparing the reaction energy barriers or the rate constants of the individual reactions. The rate ratio, ν'_{eff}/ν_{un}, listed in Table 1 shows that the reaction with the H_2SO_4 catalytic channel is 11−15 orders of magnitude faster than the reaction without H_2SO_4. As a result, H_2SO_4 could efficiently make the CH_2O hydrolysis process more feasible than the uncatalyzed channel, both energetically and kinetically. Master equation calculations are also carried out to estimate the rate coefficients of the $(H_2SO_4)(H_2O)$ + CH_2O reaction at 253−298 K and 1 atm, which were then used to calculate the overall rate expressions in Text S2 in the SI. The overall rates of sulfuric acid-catalyzed $CH_2(OH)_2$ formation obtained by RRKM theory with MESMER are slightly larger than those obtained with the TST method, as shown in Table S2 in the SI, which also indicates that it is feasible to choose the TST method to calculate the rate coefficient.

The competition between the two reactions, $CH_2O + H_2O$ and CH_2O + OH, is also investigated to evaluate the contributions of the two pathways to CH_2O elimination. Besides photolysis, the latter reaction is generally considered the dominant loss process of CH_2O in the daytime. The rate ratio between the two reactions is expressed as eq 16

$$\frac{\nu'_{eff}}{\nu_{OH}} = \frac{k'_{eff}[H_2O][CH_2O]}{k_{OH} \times [OH][CH_2O]} = \frac{K_{(H_2SO_4)(H_2O)} \times k_9 \times [H_2SO_4][H_2O]}{k_{OH} \times [OH]} \quad (16)$$

where k_{OH} is the experimental rate constant of CH_2O + OH in the atmosphere.[76] Because H_2SO_4 is formed mainly from SO_2 + OH, $[H_2SO_4]$ is low when [OH] is low. The concentrations of OH radicals and H_2O are 10^3−10^6 and 10^{18} molecules cm^{-3} (100% RH), respectively.[77,78] When [OH] = 10^5 molecules cm^{-3} and $[H_2SO_4]$ = 10^7 molecules cm^{-3}, the CH_2O hydrolysis reaction is predicted to be slower than the CH_2O + OH reaction by 2−3 orders of magnitude at 253−298 K. Because CH_2O photolysis is more advantageous than its reaction with the OH in the atmosphere, we did not further compare CH_2O hydrolysis to its photolysis. However, according to ν'_{eff}/ν_{OH}, the gas-phase hydrolysis of formaldehyde catalyzed by sulfuric acid may play a role in the sink of CH_2O at low temperatures.

3.2. Cluster Structures and Thermodynamics. To elucidate the effect of $CH_2(OH)_2$ on sulfuric acid nucleation, structures and thermodynamic values when one to three $CH_2(OH)_2$ molecules and one to three H_2SO_4 molecules formed clusters are discussed in this section. In addition, thermodynamic values were determined for the cluster formation involving the H_2SO_4 molecule and NH_3/H_2SO_4 molecule to compare with the hydrolysis product. The cluster formation steps with optimized structures of global Gibbs free energy minima in the $(H_2SO_4)_m(CH_2(OH)_2)_n$ (m = 1−3, n = 1−3) system are shown in Figure 2.

https://doi.org/10.1021/acsomega.3c00770
ACS Omega 2023, 8, 15467−15478

Table 2. Enthalpies, Entropies, and Gibbs Free Energy Changes Associated with the Affinities of the Hydrolysis Product of CH_2O to Sulfuric Acid Calculated at the DLPNO-CCSD(T)/aug-cc-pVTZ//PW91PW91/6-311++G(3df, 3pd) Level of Theory, 298.15 K and 1 atm

reactions	ΔH (kcal mol^{-1})	ΔS (cal mol^{-1} K^{-1})	ΔG (kcal mol^{-1})
$H_2SO_4 + CH_2(OH)_2 \rightleftharpoons (H_2SO_4)(CH_2(OH)_2)$	−14.85	−36.42	−3.99
$H_2SO_4 + CH_2O \rightleftharpoons (H_2SO_4)(CH_2O)$	−10.65	−30.81	−1.46
$H_2SO_4 + H_2O \rightleftharpoons (H_2SO_4)(H_2O)$	−10.93	−33.19	−1.04
$H_2SO_4 + NH_3 \rightleftharpoons (H_2SO_4)(NH_3)$	−19.49	−31.96	−9.96
$H_2SO_4 + H_2SO_4 \rightleftharpoons (H_2SO_4)_2$	−17.03	−35.65	−6.40

Table 3. Enthalpies, Entropies, and Gibbs Free Energy Changes Associated with the Affinities of Methanediol from CH_2O Hydrolysis to Sulfuric Acid Polymer Calculated at the DLPNO-CCSD(T)/aug-cc-pVTZ//PW91PW91/6-311++G(3df,3pd) Level, 298.15 K, and 1 atm

reactions	ΔH (kcal mol^{-1})	ΔS (cal mol^{-1} K^{-1})	ΔG (kcal mol^{-1})
$(H_2SO_4)_2 + CH_2(OH)_2 \rightleftharpoons (H_2SO_4)_2(CH_2(OH)_2)$	−20.92	−52.23	−5.34
$(H_2SO_4)_2 + CH_2O \rightleftharpoons (H_2SO_4)_2(CH_2O)$	−11.19	−31.63	−1.75
$(H_2SO_4)_2 + H_2O \rightleftharpoons (H_2SO_4)_2(H_2O)$	−12.58	−38.41	−1.13
$(H_2SO_4)_2 + NH_3 \rightleftharpoons (H_2SO_4)_2(NH_3)$	−28.94	−40.85	−16.76
$(H_2SO_4)_2 + H_2SO_4 \rightleftharpoons (H_2SO_4)_3$	−18.42	−47.30	−4.32
$(H_2SO_4)_3 + CH_2(OH)_2 \rightleftharpoons (H_2SO_4)_3(CH_2(OH)_2)$	−16.64	−38.26	−5.23
$(H_2SO_4)_3 + CH_2O \rightleftharpoons (H_2SO_4)_3(CH_2O)$	−12.52	−30.96	−3.29
$(H_2SO_4)_3 + H_2O \rightleftharpoons (H_2SO_4)_3(H_2O)$	−12.49	−34.13	−2.31
$(H_2SO_4)_3 + NH_3 \rightleftharpoons (H_2SO_4)_3(NH_3)$	−30.43	−32.88	−20.63
$(H_2SO_4)_3 + H_2SO_4 \rightleftharpoons (H_2SO_4)_4$	−18.32	−42.27	−5.72

The cluster formation between an SA molecule and a $CH_2(OH)_2$ molecule involves the formation of two hydrogen bonds, where $CH_2(OH)_2$ acts as both a donor and acceptor of hydrogen bonds, as shown in Figure 2. The Gibbs free energy for forming the $(H_2SO_4)(CH_2(OH)_2)$ cluster is found to be −3.99 kcal mol^{-1}. This process is more favorable than the formation of $(H_2SO_4)(CH_2O)$, with a Gibbs free energy change of −1.46 kcal mol^{-1}, as shown in Table 2. The formation of $(H_2SO_4)(CH_2(OH)_2)$ is also more favorable than that of $(H_2SO_4)(H_2O)$, with a calculated ΔG of −1.04 kcal mol^{-1}.[79] However, it is less favorable than the formation of the SA dimer, with a ΔG of −6.40 kcal mol^{-1}, and significantly less favorable than the formation of $(H_2SO_4)(NH_3)$. This result infers that the simple geminal diol is stronger for stabilizing SA to promote atmospheric particle nucleation than the simple aldehyde; however, the interaction of methanediol with SA is still weaker than that of ammonia.

The two subsequent additions of sulfuric acid molecules to the $(H_2SO_4)(CH_2(OH)_2)$ complex occur via the formation of SA−SA hydrogen-bonded interactions. These processes are found to be more favorable (i.e., −7.75 and −4.21 kcal mol^{-1}) compared to the first SA addition, which is because the addition of a sulfuric acid molecule leads to a greater reduction in the enthalpy (ΔH), although the clustering process is accompanied by an entropy (ΔS) decrease[3] as the formation of hydrogen bonds leads to a more constrained structure. From the molecular structures of these clusters, it is apparent that the interaction strengths are as follows: sulfuric acid−sulfuric acid > methanediol−sulfuric acid > methanediol−methanediol.

Formation of the $(H_2SO_4)_2(CH_2(OH)_2)_2$ cluster could occur by adding an SA molecule to $(H_2SO_4)(CH_2(OH)_2)_2$ or adding a methanediol molecule to $(H_2SO_4)_2(CH_2(OH)_2)$. Because the formation of $(H_2SO_4)_2(CH_2(OH)_2)$ is more favorable than the formation of $(H_2SO_4)(CH_2(OH)_2)_2$, where the corresponding Gibbs free energy changes from $(H_2SO_4)_2(CH_2(OH)_2)$ are −7.75 and −2.59 kcal mol^{-1}, respectively, the $(H_2SO_4)_2(CH_2(OH)_2)_2$ cluster would be formed along $(H_2SO_4)(CH_2(OH)_2) \rightarrow (H_2SO_4)_2(CH_2(OH)_2) \rightarrow (H_2SO_4)_2(CH_2(OH)_2)_2$ path. Similarly, the $(H_2SO_4)_3(CH_2(OH)_2)_3$ cluster would be formed along $(H_2SO_4)(CH_2(OH)_2) \rightarrow (H_2SO_4)_2(CH_2(OH)_2) \rightarrow (H_2SO_4)_3(CH_2(OH)_2) \rightarrow (H_2SO_4)_3(CH_2(OH)_2)_2 \rightarrow (H_2SO_4)_3(CH_2(OH)_2)_3$ path. This does not mean that $(H_2SO_4)_3(CH_2(OH)_2)_3$ cluster formation is not impossible through the $(H_2SO_4)_2(CH_2(OH)_2)_2$ cluster, since the paths are in competition with each other, and there is an actual channel occupancy (growth flux). In the following simulations of steady-state formation rates, growth fluxes were considered. For the same reactant, $(H_2SO_4)_2(CH_2(OH)_2)_2$, the addition of an SA molecule is also more favorable than the addition of a methanediol molecule, where the corresponding Gibbs free energy changes are −6.12 and −3.28 kcal mol^{-1}, respectively. Looking at the molecular structures of these clusters, the pattern is also due to the different interaction strength levels between molecules. All optimized Cartesian coordinates of $(H_2SO_4)_m(CH_2(OH)_2)_n$ ($0 \le m, n \le 3$), $(H_2SO_4)_m(H_2O)$ ($0 \le m \le 3$) and $(H_2SO_4)_m(NH_3)$ ($0 \le m \le 3$) discussed here are shown in Table S3 in the SI. The optimized structures of global Gibbs free energy minima and the corresponding optimized Cartesian coordinates for $(H_2SO_4)_m(CH_2O)_n$ ($0 \le m, n \le 3$) clusters are shown in Figure S2 and Table S4 in the SI, respectively.

In addition to examining the cluster formation between the sulfuric acid monomer and hydrolysis product of formaldehyde, we also further investigated the affinity of methanediol to dimers and trimers of sulfuric acid. Enthalpies, entropies, and Gibbs free energy changes for the corresponding reaction are shown in Table 3. Similar to the reaction between

https://doi.org/10.1021/acsomega.3c00770
ACS Omega 2023, 8, 15467−15478

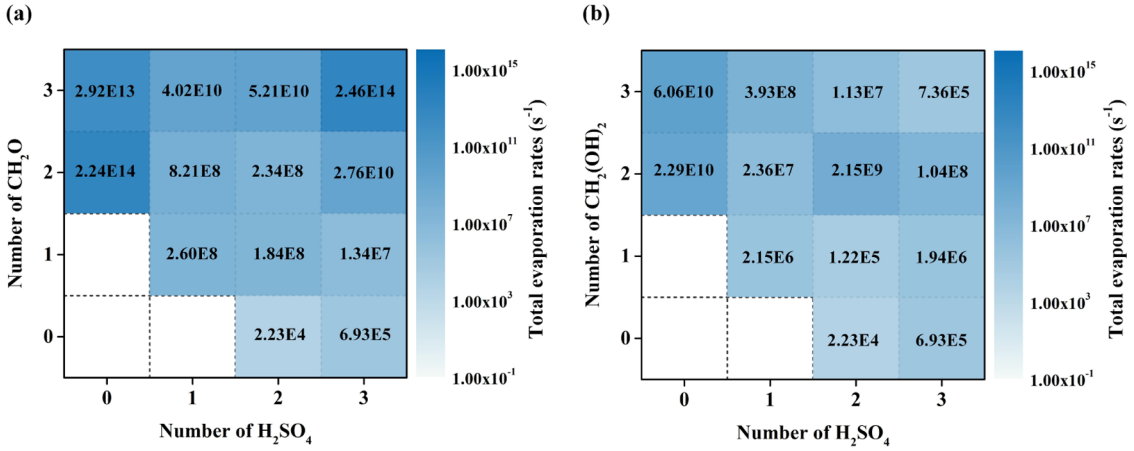

Figure 3. Total evaporation rates for the $(H_2SO_4)_m(CH_2O)_n$ ($0 \le m, n \le 3$) clusters in figure (a) and $(H_2SO_4)_m(CH_2(OH)_2)_n$ ($0 \le m, n \le 3$) clusters in (b) at the DLPNO-CCSD(T)/aug-cc-pVTZ//PW91PW91/6-311++G(3df,3pd) level of theory and 278 K.

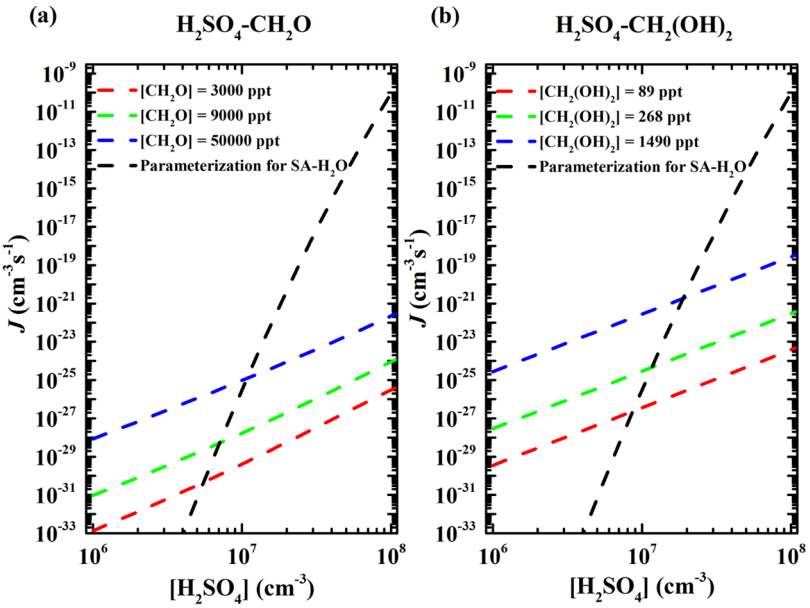

Figure 4. Simulated particle formation rate J (cm^{-3} s^{-1}) out of the simulation system as a function of H_2SO_4 monomer concentration at 278 K with different B mixing ratios for H_2SO_4-CH_2O system in figure (a) and H_2SO_4-$CH_2(OH)_2$ system in figure (b). The dashed black lines show the prediction calculated using the parameterized binary homogeneous nucleation of sulfuric acid and water at 278 K and RH = 38%.

methanediol and sulfuric acid, the methanediol affinity to sulfuric acid dimer/sulfuric acid trimer, with a value of −5.34/−5.23 kcal mol^{-1}, is higher than formaldehyde affinity; however, it is much less than the corresponding ammonia affinity. In addition, the methanediol affinities to sulfuric acid dimer and sulfuric acid trimer are similar to those of sulfuric acid itself, with values of −4.32 and −5.72 kcal mol^{-1}. All methanediol affinities to sulfuric acid, sulfuric acid dimer, and sulfuric acid trimer are higher than those corresponding to water affinities. Here, it once again proves that the simple geminal diol is stronger for stabilizing sulfuric acid and its dimer/trimer to promote nucleation than simple aldehydes. In conclusion, hydrolysis of formaldehyde can apparently enhance the binding strength with the atmospheric nucleation precursor of sulfuric acid and its dimer/trimer by introducing two functional groups (−OH groups). Formaldehyde and its atmospheric derivatives are unlikely to serve as key species, such as ammonia and amines, to promote atmospheric nucleation.

3.3. Atmospheric Cluster Dynamics Simulation.

3.3.1. Evaporation Rates. The competition between the forward reaction by adding a molecule and the reverse reaction by losing a molecule (evaporation) at each intermediate step determines whether a cluster grows to form a nanoparticle, and the collision and evaporation rates can be used to infer the stability of clusters. The total evaporation rates for the $(H_2SO_4)_m(B)_n$ ($0 \le m, n \le 3$); "B" represents CH_2O or $CH_2(OH)_2$ clusters on the H_2SO_4-B grid at 278 K are shown in Figure 3. While the evaporation rates for clusters vary between the different systems, the evaporation rates for most $(H_2SO_4)_m(CH_2O)_n$ ($0 \le m, n \le 3$) clusters are larger than that for the $(H_2SO_4)_m(CH_2(OH)_2)_n$ ($0 \le m, n \le 3$) clusters. This indicates that $(H_2SO_4)_m(CH_2(OH)_2)_n$ ($0 \le m, n \le 3$) clusters are more stable than those CH_2O-involved clusters. It is also obvious that most clusters with a higher number of H_2SO_4 molecules in these two systems have a lower evaporation rate.

https://doi.org/10.1021/acsomega.3c00770
ACS Omega 2023, 8, 15467−15478

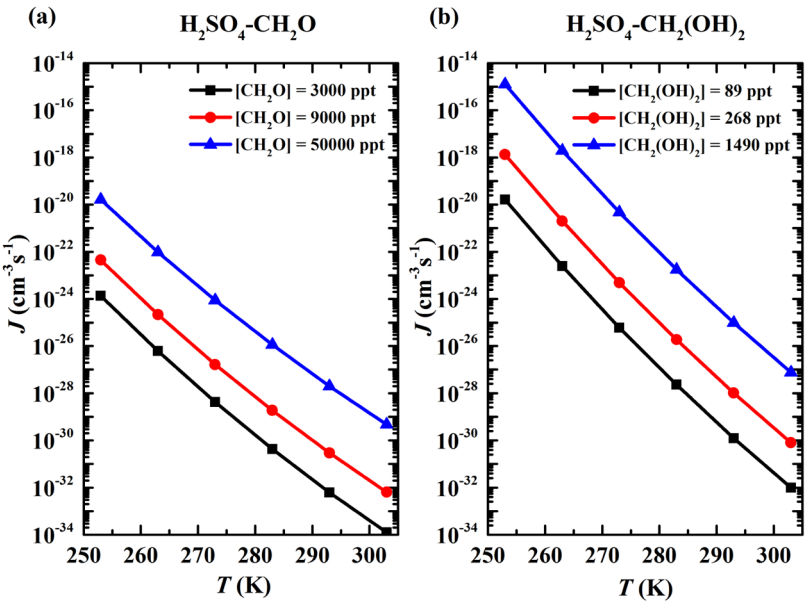

Figure 5. Simulated steady-state formation rate J (cm^{-3} s^{-1}) as a function of temperature at $[H_2SO_4] = 10^7$ molecules cm^{-3} with different B mixing ratios for H_2SO_4-CH_2O system in panel (a) and H_2SO_4-$CH_2(OH)_2$ system in panel (b).

As shown in Figure 3, the smaller evaporation rate occurs in the formation of a sulfuric acid dimer, followed by the addition of sulfuric acid in the H_2SO_4-CH_2O system. For the H_2SO_4-$CH_2(OH)_2$ system, the main path is added a SA molecule first and then added a $CH_2(OH)_2$ molecule. In general, the total evaporation rates for the $(H_2SO_4)_m(CH_2O)_n$ ($0 \le m, n \le 3$) and $(H_2SO_4)_m(CH_2(OH)_2)_n$ ($0 \le m, n \le 3$) clusters are high. It is thereby unlikely that B and SA by themselves drive new particle formation at 278 K and likely that the participation of other atmospheric vapors or other conditions is needed. The effect of the nucleating precursor concentration and temperature on the particle formation rate will be discussed next. For other atmospheric vapors, such as water vapor, it is reported that hydration[80−84] can contribute to lowering the formation Gibbs free energies of the clusters, and it is observed that particle growth increases with decreasing relative humidity using 2,4-hexadienal with H_2SO_4 as nucleation mode nanoparticles by nano-TDMA.[85] For instance, Shi et al.[35] showed that the Gibbs free energy associated with the formation of hydrated $(H_2SO_4)(P1)(H_2O)$ from $(H_2SO_4)(H_2O)$ and 3-hydroxybutyraldehyde (P1) is more negative than the Gibbs free energy of $(H_2SO_4)(P1)$ formation from H_2SO_4 and P1.

3.3.2. Steady-State Formation Rates. To form new particles, the collision rate of monomers to the clusters must exceed the cluster evaporation rates beyond some cluster size. Figure 4 shows the steady-state formation rate of particles growing out of the simulation systems as a function of monomer concentration at 278 K for H_2SO_4-CH_2O and H_2SO_4-$CH_2(OH)_2$ systems. ACDC simulations were performed at ambient SA concentrations starting from 10^6 to 10^8 molecules cm^{-3}. Because diols are difficult to isolate under typical gas-phase laboratory conditions,[86] atmospheric concentrations of $CH_2(OH)_2$ have not been achieved thus far. We computed the concentration from the equilibrium constant of formaldehyde hydrolysis, the concentration of formaldehyde and water vapor as $K_{eq}[CH_2O][H_2O]$, with $K_{eq} = (c_{ref})^{-1} \exp(-\Delta G/RT)$, based on the formation Gibbs free energy at the DLPNO-CCSD(T)/aug-cc-pVTZ//PW91PW91/6-311++G(3df, 3pd) level of theory. Concentrations of $CH_2(OH)_2$ at equilibrium with different atmospheric concentrations of formaldehyde are shown in Table S5 (SI). Our results are also accompanied by a theoretical prediction of binary homogeneous nucleation of sulfuric acid and water calculated at 278 K and 38% relative humidity (RH) according to the parameterization suggested by Vehkamäki et al.[87]

Generally, the cluster formation rate increases with increasing concentrations of B and SA under the considered conditions. The sulfuric acid concentration dependence of the cluster formation rate does not change with $CH_2(OH)_2$ and CH_2O concentrations, with a power dependency of 3 and 4, respectively; conversely, the power dependency on $CH_2(OH)_2$ does not change with SA concentration, with a value of approximately 4. Overall, the formation rates of the H_2SO_4-$CH_2(OH)_2$ system at the corresponding concentration conditions are 2−3 orders of magnitude greater than those of the H_2SO_4-CH_2O system, and all of the values are low, which again proves that the direct involvement of CH_2O in sulfuric acid and water nucleation is negligible. However, the atmospheric $CH_2(OH)_2$ concentration should actually be higher than the calculated one because there may be other ways of $CH_2(OH)_2$ production in the atmosphere. Furthermore, when the SA concentration is less than 2×10^7 molecules cm^{-3}, the formation rate is higher than that of SA and water, indicating that the cluster formation for SA with $CH_2(OH)_2$ is more favorable than that with water at ambient low SA concentrations and low RHs.

3.3.3. Effect of Temperature on Formation Rates. Temperature effects contributed to not only the thermodynamic properties of clusters,[88−91] such as enthalpy, Gibbs free energy, and conformational population, but also to kinetic parameters, such as the collision coefficient and evaporation coefficient. Thus, temperature influences the steady-state formation rate in the atmosphere by directly affecting both the Gibbs free energy change and kinetic parameters. Specifically, the cluster formation Gibbs free energy change is more negative at lower temperatures due to a negative change in the entropy, and the evaporation coefficient is also smaller at lower temperatures, which is favorable for steady-

https://doi.org/10.1021/acsomega.3c00770
ACS Omega 2023, 8, 15467−15478

state formation; however, the gas reactants will be more likely to collide and react at higher temperatures. To quantify this temperature-dependent behavior, the new particle formation rates were simulated at temperatures from 253 to 303 K with 10 K intervals, corresponding to the temperature conditions from the lower troposphere to the boundary layer.[92] Figure 5 shows the temperature-dependent behavior of the steady-state formation rates for H_2SO_4-CH_2O and H_2SO_4-$CH_2(OH)_2$ systems with $[H_2SO_4] = 1 \times 10^7$ molecules cm^{-3}.

As shown in Figure 5, the formation rate presents a negative temperature dependence in the range of 253−303 K. The formation of SA−B clusters decreases drastically with increasing temperature because the decreased Gibbs free energy change at higher temperatures and increased evaporation rate of clusters at higher temperatures reduce the formation rate, although the increased collision coefficient enhances the formation rate. The stronger bound systems are more sensitive to the temperature depicted in the order of H_2SO_4-$CH_2(OH)_2$ > H_2SO_4-CH_2O, where J values span 12 and 10 orders of magnitude, respectively.

4. CONCLUSIONS

Aldehydes were speculated to be important precursor species in the NPF, and hydrolysis of formaldehyde introduces functional groups of −OH and would have lower vapor pressure; therefore the hydrolysis product is thought to participate in NPF in the gas phase. The kinetics of CH_2O hydrolysis to produce $CH_2(OH)_2$ was examined, and the potential role of $CH_2(OH)_2$ in sulfuric acid-driven new particle formation in the atmosphere was explored. Structures and thermodynamics up to the cluster size of $(H_2SO_4)_3(B)_3$ are studied, and geometries and ΔG values calculated at 298.15 K and 1 atm show that the product derived from aldehyde hydrolysis reaction likely stabilize sulfuric acid and its dimer/trimer better than formaldehyde.

Our study serves as the first kinetic investigation of clusters containing SA and hydrolysate of formaldehyde. Formation Gibbs free energy surfaces and steady-state formation rates were calculated. In general, cluster formation for H_2SO_4 with $CH_2(OH)_2$ is more favorable than that for H_2SO_4 with CH_2O and is more favorable than that with water at ambient low H_2SO_4 concentrations and low RHs. In addition, we found that the formation rate presents a negative temperature dependence and depends exponentially on the Gibbs free energy of formation. However, the growth of SA−B clusters is essentially limited by a weak formation of the largest clusters studied. Thus, neither formaldehyde nor its atmospheric hydrolysate with sulfuric acid alone can drive the observed new particle formation events. Other stabilizing vapors are required in sulfuric acid-driven new particle formation in the atmosphere.

Higher levels of aldehydes and dicarbonyls have been shown to contribute to the growth of secondary organic aerosols.[85,93] Recently, Shi et al.[35] showed that hydrates of glyoxal are energetically favored to form hydrogen bonds with sulfuric acid and, particularly, the ΔG value of (H_2SO_4)(glyoxal) cluster formation is very close to that of $(H_2SO_4)(NH_3)$. In view of the rich content of carbonyls and different carbonyls showing different capabilities to participate in new particle formation, the role of higher aldehydes and dicarbonyls in atmospheric particle nucleation and further growth deserves further study.

ASSOCIATED CONTENT

Supporting Information

The Supporting Information is available free of charge at https://pubs.acs.org/doi/10.1021/acsomega.3c00770.

All Cartesian coordinates of optimized global Gibbs free energy minima for $(H_2SO_4)_m(B)_n$ ($0 \le m, n \le 3$; "B" represents CH_2O and $CH_2(OH)_2$), $(H_2SO_4)_m(H_2O)$ ($0 \le m \le 3$), $(H_2SO_4)_m(NH_3)$ ($0 \le m \le 3$), equilibrium geometries of the most stable conformers of $(H_2SO_4)_m(CH_2O)_n$ ($0 \le m, n \le 3$), master equation calculations, and concentrations of $CH_2(OH)_2$ at equilibrium (PDF)

AUTHOR INFORMATION

Corresponding Author

Shuai Jiang − *School of Information Science and Technology, University of Science and Technology of China, Hefei 230026 Anhui, China;* orcid.org/0000-0001-8015-4453; Email: shuaijiang@ustc.edu.cn

Authors

Chunyu Wang − *School of Biological and Environmental Engineering, Chaohu University, Hefei 238024 Anhui, China; Water Environment Research Center, Chaohu University, Hefei 238024 Anhui, China*

Xiaoju Chen − *School of Biological and Environmental Engineering, Chaohu University, Hefei 238024 Anhui, China*

Yirong Liu − *School of Information Science and Technology, University of Science and Technology of China, Hefei 230026 Anhui, China;* Present Address: Public Experimental Teaching Center, Panzhihua University, Panzhihua, Sichuan 617000, China

Teng Huang − *Laboratory of Atmospheric Physico-Chemistry, Anhui Institute of Optics & Fine Mechanics, Chinese Academy of Sciences, Hefei 230031 Anhui, China*

Complete contact information is available at: https://pubs.acs.org/10.1021/acsomega.3c00770

Notes

The authors declare no competing financial interest.

ACKNOWLEDGMENTS

This work was supported by the National Natural Science Foundation of China (Grant Nos. 42107112, 41775112, and 41877305), Chaohu University for the Start-Up grant (Grant No. KYQD-202215) and The Project of Chaohu University (Grant No. kj21kctd03).

REFERENCES

(1) Bianchi, F.; Tröstl, J.; Junninen, H.; Frege, C.; Henne, S.; Hoyle, C. R.; Molteni, U.; Herrmann, E.; Adamov, A.; Bukowiecki, N.; et al. New particle formation in the free troposphere: A question of chemistry and timing. *Science* **2016**, *352*, 1109−1112.

(2) Hanson, D. R.; Eisele, F. L. Measurement of prenucleation molecular clusters in the NH_3, H_2SO_4, H_2O system. *J. Geophys. Res.* **2002**, *107*, AAC 10-1−AAC 10-18.

(3) Zhang, R.; Khalizov, A.; Wang, L.; Hu, M.; Xu, W. Nucleation and growth of nanoparticles in the atmosphere. *Chem. Rev.* **2012**, *112*, 1957−2011.

(4) Kuang, C.; Chen, M.; Zhao, J.; Smith, J.; McMurry, P. H.; Wang, J. Size and time-resolved growth rate measurements of 1 to 5 nm freshly formed atmospheric nuclei. *Atmos. Chem. Phys.* **2012**, *12*, 3573−3589.

(5) Tröstl, J.; Chuang, W. K.; Gordon, H.; Heinritzi, M.; Yan, C.; Molteni, U.; Ahlm, L.; Frege, C.; Bianchi, F.; Wagner, R.; et al. The role of low-volatility organic compounds in initial particle growth in the atmosphere. *Nature* **2016**, *533*, 527−531.
(6) Elm, J.; Jen, C. N.; Kurtén, T.; Vehkamaki, H. Strong hydrogen bonded molecular interactions between atmospheric diamines and sulfuric acid. *J. Phys. Chem. A* **2016**, *120*, 3693−3700.
(7) Xie, H. B.; Elm, J.; Halonen, R.; Myllys, N.; Kurten, T.; Kulmala, M.; Vehkamaki, H. Atmospheric fate of monoethanolamine: Enhancing new particle formation of sulfuric acid as an important removal process. *Environ. Sci. Technol.* **2017**, *51*, 8422−8431.
(8) Roldin, P.; Ehn, M.; Kurtén, T.; Olenius, T.; Rissanen, M. P.; Sarnela, N.; Elm, J.; Rantala, P.; Hao, L.; Hyttinen, N.; et al. The role of highly oxygenated organic molecules in the Boreal aerosol-cloud-climate system. *Nat. Commun.* **2019**, *10*, No. 4370.
(9) Elm, J. Clusteromics I: Principles, Protocols, and applications to sulfuric acid−base cluster formation. *ACS Omega* **2021**, *6*, 7804−7814.
(10) Fang, X.; Hu, M.; Shang, D.; Tang, R.; Shi, L.; Olenius, T.; Wang, Y.; Wang, H.; Zhang, Z.; Chen, S.; et al. Observational evidence for the involvement of dicarboxylic acids in particle nucleation. *Environ. Sci. Technol. Lett.* **2020**, *7*, 388−394.
(11) Anderson, L. G.; Lanning, J. A.; Barrell, R.; Miyagishima, J.; Jones, R. H.; Wolfe, P. Sources and sinks of formaldehyde and acetaldehyde: An analysis of Denver's ambient concentration data. *Atmos. Environ.* **1996**, *30*, 2113−2123.
(12) Possanzini, M.; Palo, V. D.; Cecinato, A. Sources and photodecomposition of formaldehyde and acetaldehyde in Rome ambient air. *Atmos. Environ.* **2002**, *36*, 3195−3201.
(13) Zheng, J.; Zhang, R.; Garzón, J. P.; Huertas, M. E.; Levy, M.; Ma, Y.; Torres-Jardón, R.; Ruiz-Suárez, L. G.; Russell, L.; Takahama, S.; et al. Measurements of formaldehyde at the U.S.- Mexico border during the Cal-Mex 2010 air quality study. *Atmos. Environ.* **2013**, *70*, 513−520.
(14) Guo, Y.; Wang, S.; Zhu, J.; Zhang, R.; Gao, S.; Saiz-Lopez, A.; Zhou, B. Atmospheric formaldehyde, glyoxal and their relations to ozone pollution under low- and high-NOx regimes in summertime Shanghai, China. *Atmos. Res.* **2021**, *258*, No. 105635.
(15) Munger, J. W.; Jacob, D. J.; Daube, B. C.; Horowitz, L. W.; Keene, W. C.; Heikes, B. G. Formaldehyde, glyoxal, and methylglyoxal in air and cloudwater at a rural mountain site in central Virginia. *J. Geophys. Res.* **1995**, *100*, 9325−9333.
(16) Matsumoto, K.; Kawai, S.; Igawa, M. Dominant factors controlling concentrations of aldehydes in rain, fog, dew water, and in the gas phase. *Atmos. Environ.* **2005**, *39*, 7321−7329.
(17) Pinxteren, D.; Plewka, A.; Hofmann, D.; Müller, K.; Kramberger, H.; Svrcina, B.; Bächmann, K.; Jaeschke, W.; Mertes, S.; Collett, J. L.; et al. Schmücke hill cap cloud and valley stations aerosol characterisation during FEBUKO (II): Organic compounds. *Atmos. Environ.* **2005**, *39*, 4305−4320.
(18) Grosjean, D. Formaldehyde and other carbonyls in los angeles ambient air. *Environ. Sci. Technol.* **1982**, *16*, 254−262.
(19) Fried, A.; McKeen, S.; Sewell, S.; Harder, J.; Henry, B.; Goldan, P.; Kuster, W.; Williams, E.; Baumann, K.; Shetter, R.; Cantrell, C. Photochemistry of formaldehyde during the 1993 Tropospheric OH Photochemistry Experiment. *J. Geophys. Res.* **1997**, *102*, 6283−6296.
(20) Iraci, L. T.; Tolbert, M. A. Heterogeneous interaction of formaldehyde with cold sulfuric acid: Implications for the upper troposphere and lower stratosphere. *J. Geophys. Res.* **1997**, *102*, 16099−16107.
(21) Zimmerman, P. R.; Chatfield, R. B.; Fishman, J.; Crutzen, P. J.; Hanst, P. L. Estimates on the production of CO and H_2 from the oxidation of hydrocarbon emissions from vegetation. *Geophys. Res. Lett.* **1978**, *5*, 679−682.
(22) Carbajo, P. G.; Smith, S. C.; Holloway, A.-L.; Smith, C. A.; Pope, F. D.; Shallcross, D. E.; Orr-Ewing, A. J. Ultraviolet photolysis of HCHO: Absolute HCO quantum yields by direct detection of the HCO radical photoproduct. *J. Phys. Chem. A* **2008**, *112*, 12437−12448.
(23) Feilberg, K. L.; D'Anna, B.; Johnson, M. S.; Nielsen, C. J. Relative Tropospheric photolysis rates of HCHO, $H^{13}CHO$, $HCH^{18}O$, and DCDO measured at the european photoreactor facility. *J. Phys. Chem. A* **2005**, *109*, 8314−8319.
(24) Alvarez-Idaboy, J. R.; Mora-Diez, N.; Boyd, R. J.; Vivier-Bunge, A. On the importance of prereactive complexes in molecule-radical reactions: Hydrogen abstraction from aldehydes by OH. *J. Am. Chem. Soc.* **2001**, *123*, 2018−2024.
(25) Hak, C.; P, I.; Trick, S.; Kern, C.; Platt, U.; Dommen, J.; Ordó -nez, C.; Prévôt, A. S. H.; Junkermann, W.; Astorga-Lloréns, C.; Larsen, B. R.; Mellqvist, J.; Strandberg, A.; Yu, Y.; Galle, B.; Kleffmann, J.; Lörzer, J. C.; Braathen, G. O.; Volkamer, R. Intercomparison of four different in-situ techniques for ambient formaldehyde measurements in urban air. *Atmos. Chem. Phys.* **2005**, *5*, 2881−2900.
(26) Atkinson, R. Atmospheric chemistry of VOCs and NOx. *Atmos. Environ.* **2000**, *34*, 2063−2101.
(27) Jacob, D. J. Heterogeneous chemistry and tropospheric ozone. *Atmos. Environ.* **2000**, *34*, 2131−2159.
(28) Wagner, V.; von Glasow, R.; Fischer, H.; Crutzen, P. J. Are CH_2O measurements in the marine boundary layer suitable for testing the current understanding of CH_4 photooxidation?: A model study. *J. Geophys. Res.* **2002**, *107*, ACH 3-1−ACH 3-14.
(29) Long, B.; Tan, X.-F.; Chang, C.-R.; Zhao, W.-X.; Long, Z.-W.; Ren, D.-S.; Zhang, W.-J. Theoretical studies on gas-phase reactions of sulfuric acid catalyzed hydrolysis of formaldehyde and formaldehyde with sulfuric acid and $H_2SO_4\cdots H_2O$ Complex. *J. Phys. Chem. A* **2013**, *117*, 5106−5116.
(30) Hazra, M. K.; Francisco, J. S.; Sinha, A. Gas phase hydrolysis of formaldehyde to form methanediol: Impact of formic acid catalysis. *J. Phys. Chem. A* **2013**, *117*, 11704−11710.
(31) Zhou, X.; Lee, Y.-N.; Newman, L.; Chen, X.; Mopper, K. Tropospheric formaldehyde concentration at the Mauna Loa Observatory during the Mauna Loa Observatory Photochemistry Experiment 2. *J. Geophys. Res.* **1996**, *101*, 14711−14719.
(32) Tie, X.; Brasseur, G.; Emmons, L.; Horowitz, L.; Kinnison, D. Effects of aerosols on tropospheric oxidants: A global model study. *J. Geophys. Res.* **2001**, *106*, 22931−22964.
(33) Fried, A.; Crawford, J.; Olson, J.; Walega, J.; Potter, W.; Wert, B.; Jordan, C.; Anderson, B.; Shetter, R.; Lefer, B.; et al. Airborne tunable diode laser measurements of formaldehyde during TRACE-P: Distributions and box model comparisons. *J. Geophys. Res.* **2003**, *108*, No. 8798.
(34) Li, G.; Su, H.; Li, X.; Kuhn, U.; Meusel, H.; Hoffmann, T.; Ammann, M.; Pöschl, U.; Shao, M.; Cheng, Y. Uptake of gaseous formaldehyde by soil surfaces: a combination of adsorption/desorption equilibrium and chemical reactions. *Atmos. Chem. Phys.* **2016**, *16*, 10299−10311.
(35) Shi, X.; Zhang, R.; Sun, Y.; Xu, F.; Zhang, Q.; Wang, W. A density functional theory study of aldehydes and their atmospheric products participating in nucleation. *Phys. Chem. Chem. Phys.* **2018**, *20*, 1005−1011.
(36) Wang, C.-Y.; Jiang, S.; Wang, Z.-Q.; Liu, Y.-R.; Wen, H.; Huang, T.; Han, Y.-J.; Huang, W. Can formaldehyde contribute to atmospheric new particle formation from sulfuric acid and water? *Atmos. Environ.* **2019**, *201*, 323−333.
(37) Jang, M.; Kamens, R. M. Atmospheric secondary aerosol formation by heterogeneous reactions of aldehydes in the presence of a sulfuric acid aerosol catalyst. *Environ. Sci. Technol.* **2001**, *35*, 4758−4766.
(38) Hawkins, L. N.; Baril, M. J.; Sedehi, N.; Galloway, M. M.; De Haan, D. O.; Schill, G. P.; Tolbert, M. A. Formation of semisolid, oligomerized aqueous SOA: Lab simulations of cloud processing. *Environ. Sci. Technol.* **2014**, *48*, 2273−2280.
(39) Williams, I. H. Theoretical modelling of specific solvation effects upon carbonyl addition. *J. Am. Chem. Soc.* **1987**, *109*, 6299−6307.

https://doi.org/10.1021/acsomega.3c00770
ACS Omega 2023, 8, 15467−15478

(40) Wolfe, S.; Kim, C.-K.; Yang, K.; Weinberg, N.; Shi, Z. Hydration of the carbonyl group. A theoretical study of the cooperative mechanism. *J. Am. Chem. Soc.* **1995**, *117*, 4240−4260.
(41) Böhm, S.; Antipova, D.; Kuthan, J. Methanediol decomposition mechanisms: A study considering various ab initio approaches. *Int. J. Quantum Chem.* **1996**, *58*, 47−55.
(42) Axson, J. L.; Takahashi, K.; De Haan, D. O.; Vaida, V. Gas-phase water-mediated equilibrium between methylglyoxal and its geminal diol. *Proc. Natl. Acad. Sci. U.S.A.* **2010**, *107*, 6687−6692.
(43) Kahan, T. F.; Ormond, T. K.; Ellison, G. B.; Vaida, V. Acetic acid formation via the hydration of gas-phase ketene under ambient conditions. *Chem. Phys. Lett.* **2013**, *565*, 1−4.
(44) Hirvonen, V.; Myllys, N.; Kurten, T.; Elm, J. Closed-shell organic compounds might form dimers at the surface of molecular clusters. *J. Phys. Chem. A* **2018**, *122*, 1771−1780.
(45) Liu, F.-Y.; Tan, X.-F.; Long, Z.-W.; Long, B.; Zhang, W.-J. New insights in atmospheric acid-catalyzed gas phase hydrolysis of formaldehyde: a theoretical study. *RSC Adv.* **2015**, *5*, 32941−32949.
(46) Rypkema, H. A.; Sinha, A.; Francisco, J. S. Carboxylic acid catalyzed hydration of acetaldehyde. *J. Phys. Chem. A* **2015**, *119*, 4581−4588.
(47) McGrath, M. J.; Olenius, T.; Ortega, I. K.; Loukonen, V.; Paasonen, P.; Kurtén, T.; Kulmala, M.; Vehkamäki, H. Atmospheric Cluster Dynamics Code: a flexible method for solution of the birth-death equations. *Atmos. Chem. Phys.* **2012**, *12*, 2345−2355.
(48) Olenius, T.; Kupiainen-Määttä, O.; Ortega, I. K.; Kurtén, T.; Vehkamäki, H. Free energy barrier in the growth of sulfuric acid-ammonia and sulfuric acid-dimethylamine clusters. *J. Chem. Phys.* **2013**, *139*, No. 084312.
(49) Yoon, J.-W.; Park, J.-H.; Shur, C.-C.; Jung, S.-B. Characteristic evaluation of electroless nickel-phosphorus deposits with different phosphorus contents. *Microelectron. Eng.* **2007**, *84*, 2552−2557.
(50) Wales, D. J.; Doye, J. P. K. Global optimization by basin-hopping and the lowest energy structures of Lennard-jones clusters containing up to 110 atoms. *J. Phys. Chem. A* **1997**, *101*, 5111−5116.
(51) Huang, W.; Pal, R.; Wang, L.-M.; Zeng, X. C.; Wang, L.-S. Isomer identification and resolution in small gold clusters. *J. Chem. Phys.* **2010**, *132*, No. 054305.
(52) Stewart, J. J. P. Optimization of parameters for semiempirical methods VI: more modifications to the NDDO approximations and re-optimization of parameters. *J. Mol. Model.* **2013**, *19*, 1−32.
(53) Huang, W.; Ji, M.; Dong, C.-D.; Gu, X.; Wang, L.-M.; Gong, X. G.; Wang, L.-S. Relativistic effects and the unique low-symmetry structures of gold nanoclusters. *ACS Nano.* **2008**, *2*, 897−904.
(54) Huang, W.; Sergeeva, A. P.; Zhai, H.-J.; Averkiev, B. B.; Wang, L.-S.; Boldyrev, A. I. A concentric planar doubly π-aromatic B19-cluster. *Nat. Chem.* **2010**, *2*, 202−206.
(55) Jiang, S.; Liu, Y. R.; Huang, T.; Wen, H.; Xu, K. M.; Zhao, W. X.; Zhang, W. J.; Huang, W. Study of Cl-(H_2O)n (n = 1-4) using basin-hopping method coupled with density functional theory. *J. Comput. Chem.* **2014**, *35*, 159−165.
(56) Liu, Y.-R.; Wen, H.; Huang, T.; Lin, X.-X.; Gai, Y.-B.; Hu, C.-J.; Zhang, W.-J.; Huang, W. Structural exploration of water, nitrate/water, and oxalate/water clusters with basin-hopping method using a compressed sampling technique. *J. Phys. Chem. A* **2014**, *118*, 508−516.
(57) Wang, C. Y.; Ma, Y.; Chen, J.; Jiang, S.; Liu, Y. R.; Wen, H.; Feng, Y. J.; Hong, Y.; Huang, T.; Huang, W. Bidirectional interaction of alanine with sulfuric acid in the presence of water and the atmospheric implication. *J. Phys. Chem. A* **2016**, *120*, 2357−2371.
(58) Wang, C.-Y.; Jiang, S.; Liu, Y.-R.; Wen, H.; Wang, Z.-Q.; Han, Y.-J.; Huang, T.; Huang, W. Synergistic effect of ammonia and methylamine on nucleation in the Earth's atmosphere. A theoretical study. *J. Phys. Chem. A* **2018**, *122*, 3470−3479.
(59) Frisch, M. J.; Schlegel, H. B.; Scuseria, G. E.; Robb, M. A.; Scalmani, G.; Barone, V.; Mennucci, B.; Petersson, G. A.; Caricato, M.; Li, X.et al. *Gaussian 09*, Revision A.02; Gaussian, Inc.: Wallingford CT., 2009.
(60) Kurtén, T.; Torpo, L.; Ding, C.-G.; Vehkamäki, H.; Sundberg, M. R.; Laasonen, K.; Kulmala, M. A density functional study on water-sulfuric acid-ammonia clusters and implications for atmospheric cluster formation. *J. Geophys. Res.* **2007**, *112*, No. D04210.
(61) Nadykto, A. B.; Yu, F.; Herb, J. Towards understanding the sign preference in binary atmospheric nucleation. *Phys. Chem. Chem. Phys.* **2008**, *10*, 7073−7078.
(62) Nadykto, A. B.; Du, H.; Yu, F. Quantum DFT and DF-DFT study of vibrational spectra of sulfuric acid, sulfuric acid monohydrate, formic acid and its cyclic dimer. *Vib. Spectrosc.* **2007**, *44*, 286−296.
(63) Nadykto, A. B.; Yu, F. Strong hydrogen bonding between atmospheric nucleation precursors and common organics. *Chem. Phys. Lett.* **2007**, *435*, 14−18.
(64) Wen, H.; Huang, T.; Wang, C.-Y.; Peng, X.-Q.; Jiang, S.; Liu, Y.-R.; Huang, W. A study on the microscopic mechanism of methanesulfonic acid-promoted binary nucleation of sulfuric acid and water. *Atmos. Environ.* **2018**, *191*, 214−226.
(65) Neese, F. Software update: the ORCA program system, version 4.0. *Wiley Interdiscip. Rev.: Comput. Mol. Sci.* **2018**, *8*, No. e1327.
(66) Zhao, Y.; Truhlar, D. G. The M06 suite of density functionals for main group thermochemistry, thermochemical kinetics, noncovalent interactions, excited states, and transition elements: two new functionals and systematic testing of four M06-class functionals and 12 other functionals. *Theor. Chem. Acc.* **2008**, *120*, 215−241.
(67) Frisch, M. J.; Pople, J. A.; Binkley, J. S. Self-consistent molecular orbital methods 25. Supplementary functions for Gaussian basis sets. *J. Chem. Phys.* **1984**, *80*, 3265−3269.
(68) Eckart, C. The penetration of a potential barrier by electrons. *Phys. Rev.* **1930**, *35*, 1303−1309.
(69) Truhlar, D. G.; Garrett, B. C.; Klippenstein, S. J. Current status of Transition-State Theory. *J. Phys. Chem. A* **1996**, *100*, 12771−12800.
(70) Canneaux, S.; Bohr, F.; Henon, E. KiSThelP: a program to predict thermodynamic properties and rate constants from quantum chemistry results. *J. Comput. Chem.* **2014**, *35*, 82−93.
(71) Fliegl, H.; Glöß, A.; Welz, O.; Olzmann, M.; Klopper, W. Accurate computational determination of the binding energy of the SO3•H2O complex. *J. Chem. Phys.* **2006**, *125*, No. 054312.
(72) Li, G.-B.; Cai, S.-H.; Long, B. New reactions for the formation of organic nitrate in the atmosphere. *ACS Omega* **2022**, *7*, 39671−39679.
(73) Epstein, S. A.; Nizkorodov, S. A. A comparison of the chemical sinks of atmospheric organics in the gas and aqueous phase. *Atmos. Chem. Phys.* **2012**, *12*, 8205−8222.
(74) Hemming, B. L.; Seinfeld, J. H. On the hygroscopic behavior of atmospheric organic aerosols. *Ind. Eng. Chem. Res.* **2001**, *40*, 4162−4171.
(75) Yang, L.; Nie, W.; Liu, Y.; Xu, Z.; Xiao, M.; Qi, X.; Li, Y.; Wang, R.; Zou, J.; Paasonen, P.; et al. Toward building a physical proxy for gas-phase sulfuric acid concentration based on its budget analysis in polluted Yangtze River Delta, East China. *Environ. Sci. Technol.* **2021**, *55*, 6665−6676.
(76) Atkinson, R.; Baulch, D. L.; Cox, R. A.; Crowley, J. N.; Hampson, R. F.; Hynes, R. G.; Jenkin, M. E.; Rossi, M. J.; Troe, J.; IUPAC Subcommittee. Evaluated kinetic and photochemical data for atmospheric chemistry: Volume II - gas phase reactions of organic species. *Atmos. Chem. Phys.* **2006**, *6*, 3625−4055.
(77) Liu, J.-Y.; Long, Z.-W.; Mitchell, E.; Long, B. New mechanistic pathways for the reactions of formaldehyde with formic acid catalyzed by sulfuric acid and formaldehyde with sulfuric acid catalyzed by formic acid: formation of potential secondary organic aerosol precursors. *ACS Earth Space Chem.* **2021**, *5*, 1363−1372.
(78) Khan, M. A. H.; Ashfold, M. J.; Nickless, G.; Martin, D.; Watson, L. A.; Hamer, P. D.; Wayne, R. P.; Canosa-Mas, C. E.; Shallcross, D. E. Night-time NO_3 and OH radical concentrations in the United Kingdom inferred from hydrocarbon measurements. *Atmos. Sci. Lett.* **2008**, *9*, 140−146.
(79) Hanson, D. R.; Eisele, F. Diffusion of H_2SO_4 in humidified nitrogen: hydrated H_2SO_4. *J. Phys. Chem. A* **2000**, *104*, 1715−1719.

https://doi.org/10.1021/acsomega.3c00770
ACS Omega 2023, 8, 15467−15478

(80) Temelso, B.; Phan, T. N.; Shields, G. C. Computational study of the hydration of sulfuric acid dimers: Implications for acid dissociation and aerosol formation. *J. Phys. Chem. A* **2012**, *116*, 9745−9758.
(81) Husar, D. E.; Temelso, B.; Ashworth, A. L.; Shields, G. C. Hydration of the bisulfate ion: atmospheric implications. *J. Phys. Chem. A* **2012**, *116*, 5151−5163.
(82) Temelso, B.; Morrell, T. E.; Shields, R. M.; Allodi, M. A.; Wood, E. K.; Kirschner, K. N.; Castonguay, T. C.; Archer, K. A.; Shields, G. C. Quantum mechanical study of sulfuric acid hydration: Atmospheric implications. *J. Phys. Chem. A* **2012**, *116*, 2209−2224.
(83) Henschel, H.; Navarro, J. C. A.; Yli-Juuti, T.; Kupiainen-Määttä, O.; Olenius, T.; Ortega, I. K.; Clegg, S. L.; Kurtén, T.; Riipinen, I.; Vehkamäki, H. Hydration of atmospherically relevant molecular clusters: Computational chemistry and classical thermodynamics. *J. Phys. Chem. A* **2014**, *118*, 2599−2611.
(84) Bustos, D. J.; Temelso, B.; Shields, G. C. Hydration of the sulfuric acid-methylamine complex and implications for aerosol formation. *J. Phys. Chem. A* **2014**, *118*, 7430−7441.
(85) Wang, L.; Khalizov, A. F.; Zheng, J.; Xu, W.; Ma, Y.; Lal, V.; Zhang, R. Atmospheric nanoparticles formed from heterogeneous reactions of organics. *Nat. Geosci.* **2010**, *3*, 238−242.
(86) Zhu, C.; Kleimeier, N. F.; Turner, A. M.; Singh, S. K.; Fortenberry, R. C.; Kaiser, R. I. Synthesis of methanediol [$CH_2(OH)_2$]: The simplest geminal diol. *Proc. Natl. Acad. Sci. U.S.A.* **2022**, *119*, No. e2111938119.
(87) Vehkamäki, H.; Kulmala, M.; Napari, I.; Lehtinen, K. E. J.; Timmreck, C.; Noppel, M.; Laaksonen, A. An improved parameterization for sulfuric acid-water nucleation rates for tropospheric and stratospheric conditions. *J. Geophys. Res.* **2002**, *107*, AAC 3-1−AAC 3-10.
(88) Kim, J.; Mhin, B. J.; Lee, S. J.; Kim, K. S. Entropy-driven structures of the water octamer. *Chem. Phys. Lett.* **1994**, *219*, 243−246.
(89) Mhin, B. J.; Lee, S. J.; Kim, K. S. Water-cluster distribution with respect to pressure and temperature in the gas phase. *Phys. Rev. A* **1993**, *48*, 3764−3770.
(90) Lee, H. M.; Suh, S. B.; Lee, J. Y.; Tarakeshwar, P.; Kim, K. S. Structures, energies, vibrational spectra, and electronic properties of water monomer to decamer. *J. Chem. Phys.* **2000**, *112*, 9759−9772.
(91) Jiang, S.; Huang, T.; Liu, Y. R.; Xu, K. M.; Zhang, Y.; Lv, Y. Z.; Huang, W. Theoretical study of temperature dependence and Rayleigh scattering properties of chloride hydration clusters. *Phys. Chem. Chem. Phys.* **2014**, *16*, 19241−19249.
(92) Sarangi, C.; Tripathi, S. N.; Mishra, A. K.; Goel, A.; Welton, E. J. Elevated aerosol layers and their radiative impact over Kanpur during monsoon onset period. *J. Geophys. Res.* **2016**, *121*, 7936−7957.
(93) Kalberer, M.; Paulsen, D.; Sax, M.; Steinbacher, M.; Dommen, J.; Prevot, A. S. H.; Fisseha, R.; Weingartner, E.; Frankevich, V.; Zenobi, R.; Baltensperger, U. Identification of polymers as major components of atmospheric organic aerosols. *Science* **2004**, *303*, 1659−1662.

https://doi.org/10.1021/acsomega.3c00770
ACS Omega 2023, 8, 15467−15478